FGF21 is required for the metabolic benefits of IKKε/TBK1 inhibition

Shannon M. Reilly,[1,2] Mohammad Abu-Odeh,[1] Magdalene Ameka,[3,4] Julia H. DeLuca,[1] Meghan C. Naber,[3,4] Benyamin Dadpey,[1] Nima Ebadat,[1] Andrew V. Gomez,[1] Xiaoling Peng,[2] BreAnne Poirier,[2] Elyse Walk,[1] Matthew J. Potthoff,[3,4] and Alan R. Saltiel[1,2]

[1]Division of Metabolism and Endocrinology, Department of Medicine, UCSD, La Jolla, California, USA. [2]Life Sciences Institute, University of Michigan, Ann Arbor, Michigan, USA. [3]Department of Neuroscience and Pharmacology and [4]Fraternal Order of Eagles Diabetes Research Center, University of Iowa Carver College of Medicine, Iowa City, Iowa, USA.

The protein kinases IKKε and TBK1 are activated in liver and fat in mouse models of obesity. We have previously demonstrated that treatment with the IKKε/TBK1 inhibitor amlexanox produces weight loss and relieves insulin resistance in obese animals and patients. While amlexanox treatment caused a transient reduction in food intake, long-term weight loss was attributable to increased energy expenditure via FGF21-dependent beiging of white adipose tissue (WAT). Amlexanox increased FGF21 synthesis and secretion in several tissues. Interestingly, although hepatic secretion determined circulating levels, it was dispensable for regulating energy expenditure. In contrast, adipocyte-secreted FGF21 may have acted as an autocrine factor that led to adipose tissue browning and weight loss in obese mice. Moreover, increased energy expenditure was an important determinant of improved insulin sensitivity by amlexanox. Conversely, the immediate reductions in fasting blood glucose observed with acute amlexanox treatment were mediated by the suppression of hepatic glucose production via activation of STAT3 by adipocyte-secreted IL-6. These findings demonstrate that amlexanox improved metabolic health via FGF21 action in adipocytes to increase energy expenditure via WAT beiging and that adipocyte-derived IL-6 has an endocrine role in decreasing gluconeogenesis via hepatic STAT3 activation, thereby producing a coordinated improvement in metabolic parameters.

Introduction

We are in the midst of a worldwide epidemic of obesity and related metabolic disorders, most notably type 2 diabetes (1–6). Obesity is a consequence of a positive energy balance due to excessive energy intake and reduced energy expenditure. Although the molecular events that control the energy balance and its link to type 2 diabetes remain uncertain, numerous studies have implicated an important role for chronic, low-grade inflammation (7–11). Indeed, both dietary and genetic obesity produces an inflammatory state in liver and fat accompanied by the appearance of proinflammatory macrophages and local secretion of cytokines and chemokines that attenuate insulin action (12–15). KO or pharmacological inhibition of inflammatory pathways in rodents can disrupt the link between genetically or diet-induced obesity and both insulin and catecholamine resistance, suggesting that local inflammation is a key step in the generation of cellular resistance to important hormones that regulate metabolism. Although the role of inflammation in human obesity is less clear, numerous studies have demonstrated a strong association between inflammatory signals, insulin resistance, and obesity (8, 9, 15–17).

The NF-κB transcriptional program is activated in obese fat and may play an important role in the development of several metabolic abnormalities (18–20). We and others have observed that the NF-κB–sensitive genes *Tbk1* and *Ikbke* are increased at both the mRNA and protein levels in adipose tissue during high-fat diet (HFD) feeding of mice, whereas *Ikbke* mRNA and protein levels and TBK1 activity are increased in liver (21–23). Moreover, global deletion of the *Ikbke* gene rendered mice partially resistant to the HFD-dependent development of obesity, insulin resistance, hepatic steatosis, and inflammation (24). Conditional deletion of *Tbk*1 in adipocytes produced mice with resistance to diet-induced obesity and improved energy expenditure by restoring AMPK activity (23). This led us to identify the IKKε/TBK1 inhibitor, amlexanox, which had been previously developed for the treatment of asthma, allergic rhinitis, and aphthous ulcers (25). Administration of this selective drug to obese mice produced reversible weight loss and improved insulin sensitivity, reduced inflammation, and attenuated hepatic steatosis (21). A placebo-controlled, double-blind randomized study of 40 patients with obesity and type 2 diabetes revealed that amlexanox treatment produced a significant 0.5% reduction in hemoglobin A1c levels and improvement in insulin sensitivity (26). Interestingly, this study identified a subset of patients with high levels of underlying inflammation, who were significantly more responsive to amlexanox. RNA-Seq analysis of gene expression patterns in adipose tissue from these patients revealed changes consistent with those observed in mice, indicating inhibition of TBK1 and IKKε activity (26).

A primary target of amlexanox in rodents is the subcutaneous adipose tissue, where it increases energy expenditure partly by

Conflict of interest: ARS is a founder of Elgia Therapeutics and is a named inventor on the following patents related to amlexanox: US Patent 8,946,424, "Deuterated amlexanox" and US Patent 10,245,255, "Composition and methods for the treatment of obesity and related disorders."

Submitted: October 28, 2020; **Accepted:** March 23, 2021; **Published:** May 17, 2021.
Reference information: *J Clin Invest*. 2021;131(10):e145546.
https://doi.org/10.1172/JCI145546.

enhancing catecholamine sensitivity via inhibition of IKKε (27) and browning of adipocytes (21). Increased IKKε expression has also been linked with catecholamine resistance in adipocytes from children with obesity (28). The increase in catecholamine sensitivity with amlexanox treatment in mice resulted in a transient increase in IL-6 synthesis and secretion from adipocytes and preadipocytes, which was responsible for acute lowering of blood sugar via reduced hepatic glucose output (29). Additionally, inhibition of TBK1 produces a marked increase in the activity of AMPK, along with decreased lipogenesis and increased mitochondrial biogenesis (23).

Here, we elucidate the mechanism by which amlexanox produced weight loss and improvements in glucose handling and insulin sensitivity. During the first week of treatment, amlexanox transiently suppressed food intake, irrespective of the route of administration of the drug. Interestingly, this suppression of food intake was not responsible for the reductions in fasting blood glucose observed with amlexanox treatment, which were instead the result of suppression of hepatic glucose production via an adipocyte-to-hepatocyte signaling axis. While food intake quickly returned to normal, amlexanox treatment continued to promote weight loss by increasing thermogenic energy expenditure. Interestingly, this increase in energy expenditure produced by amlexanox required the synthesis of both UCP1 and FGF21 in adipocytes. FGF21 may operate as an autocrine factor in adipocytes, delivering a necessary second signal in response to catecholamine signaling to generate a thermogenic program that includes the induction of *Ucp1* and other genes. FGF21-dependent weight loss appeared to be a major contributing factor for the improvements in insulin sensitivity observed with amlexanox treatment, suggesting that inhibition of TBK1 and IKKε in adipocytes may represent an effective strategy for increasing adipose FGF21 to deliver specific therapeutic benefits.

Results

Amlexanox treatment causes transient hypophagia. As previously reported (21), treatment of diet-induced obese mice with 25 mg/kg amlexanox by daily oral gavage produced significant weight loss over a 4-week period (Figure 1A). To examine the mechanism of weight loss, we placed animals in a metabolic cage to measure food intake and energy expenditure for 2 baseline days followed by 3 days of amlexanox or vehicle control treatment. We previously demonstrated that 4 weeks of amlexanox treatment increased energy expenditure in concordance with increased thermogenic gene expression in subcutaneous white adipose tissue (WAT), characteristic of adipose tissue browning (21). We were surprised to observe that acute amlexanox treatment resulted in reduced energy expenditure during the dark cycle, as evidenced by a decrease in the oxygen consumption and carbon dioxide production rates (Figure 1, B–E). Evaluation of food intake revealed that acute amlexanox treatment resulted in a significant reduction in food intake during this period (Figure 1F).

Our previous studies on the prevention of obesity by amlexanox (treatment initiated at the same time as the HFD) found no acute suppression of food intake (21), indicating that this effect is limited to obese animals. We also demonstrated that acute amlexanox treatment results in a robust increase in circulating IL-6 (29). Since IL-6 has previously been suggested to induce hypophagia similarly to leptin (30–32), we examined food intake in HFD-fed *Il6*-KO mice treated with amlexanox. We observed equal reductions in food intake with amlexanox treatment in *Il6*-KO and littermate WT control mice (Figure 1G), indicating that acute amlexanox-induced hypophagia was not mediated by IL-6 or its downstream targets.

Amlexanox has an excellent safety record in both mice and humans (23, 26, 33, 34). Nevertheless, we wanted to examine the possibility that the hypophagic response to amlexanox was the result of illness-like behavior due to acute inflammation. During acute-phase inflammation, it is common to see increased levels of the inflammatory cytokines TNF-α and IL-1α as well as IL-6. Unlike IL-6, neither TNF-α nor IL-1α was induced by amlexanox treatment (Supplemental Figure 1, A–C; supplemental material available online with this article; https://doi.org/10.1172/JCI145546DS1). In fact, after 2 weeks of treatment, we detected a significant reduction in serum TNF-α levels, consistent with previous observations that long-term amlexanox treatment reduces inflammation (21). Additionally, no induction of the chemokines MCP1 (aka CCL2), MIP1α (aka CCL3), or RANTES (aka CCL5), often associated with adipose tissue inflammation, was observed with amlexanox treatment (Supplemental Figure 1, D–F). These data suggest that the induction of IL-6 is a specific metabolic response in adipocytes and is not indicative of an acute inflammatory response to amlexanox treatment.

To understand the contribution of hypophagia to weight loss in obese animals treated with amlexanox, we measured daily food intake over the first 2 weeks of treatment. A significant reduction in food intake was only observed during the first 3 days of treatment (Figure 1, H and I). Differences in food intake after the third day of treatment were not significant after correction for multiple comparisons. We observed no difference in food intake in the second week of treatment and beyond, consistent with our previous observation that food intake in obese mice was equal once the animals reach maximal weight loss, after 4 weeks of amlexanox treatment (21). The reduction in food intake was associated with weight loss over the first 3 days of amlexanox treatment (Figure 1, J and K). However, the amlexanox-treated animals continued to lose weight during the second week of treatment when food intake was equal to that of the vehicle control mice, indicating that amlexanox also produced weight loss via a food intake–independent mechanism (Figure 1, J and K). Additionally, the reduction in food intake was not due to the oral route of drug administration, as intraperitoneal injection with amlexanox produced the same transient reduction in food intake and pattern of weight loss (Supplemental Figure 2).

Amlexanox treatment increases energy expenditure. To determine the mechanism by which amlexanox modulates energy expenditure independent of effects on food intake, we repeated the metabolic cage study with paired feeding. Food access for the vehicle-treated animals was limited, such that these animals were only allowed to consume the same amount of food as the amlexanox-treated animals (Figure 2A and Supplemental Figure 3, A and B). The animals were acclimated to the cage for 1 dark cycle before treatment initiation. Prior to treatment, both groups of animals exhibited the same level of foraging activity as determined by *z*-axis beam breaks (Figure 2, B and C). Consistent with the reduction in food intake, amlexanox treatment significantly reduced foraging activity relative to baseline, whereas no change was observed in the pair-fed, vehicle-treated control group (Figure 2, B and C). On the first and second night after treatment initiation, pair-fed, vehicle-treated

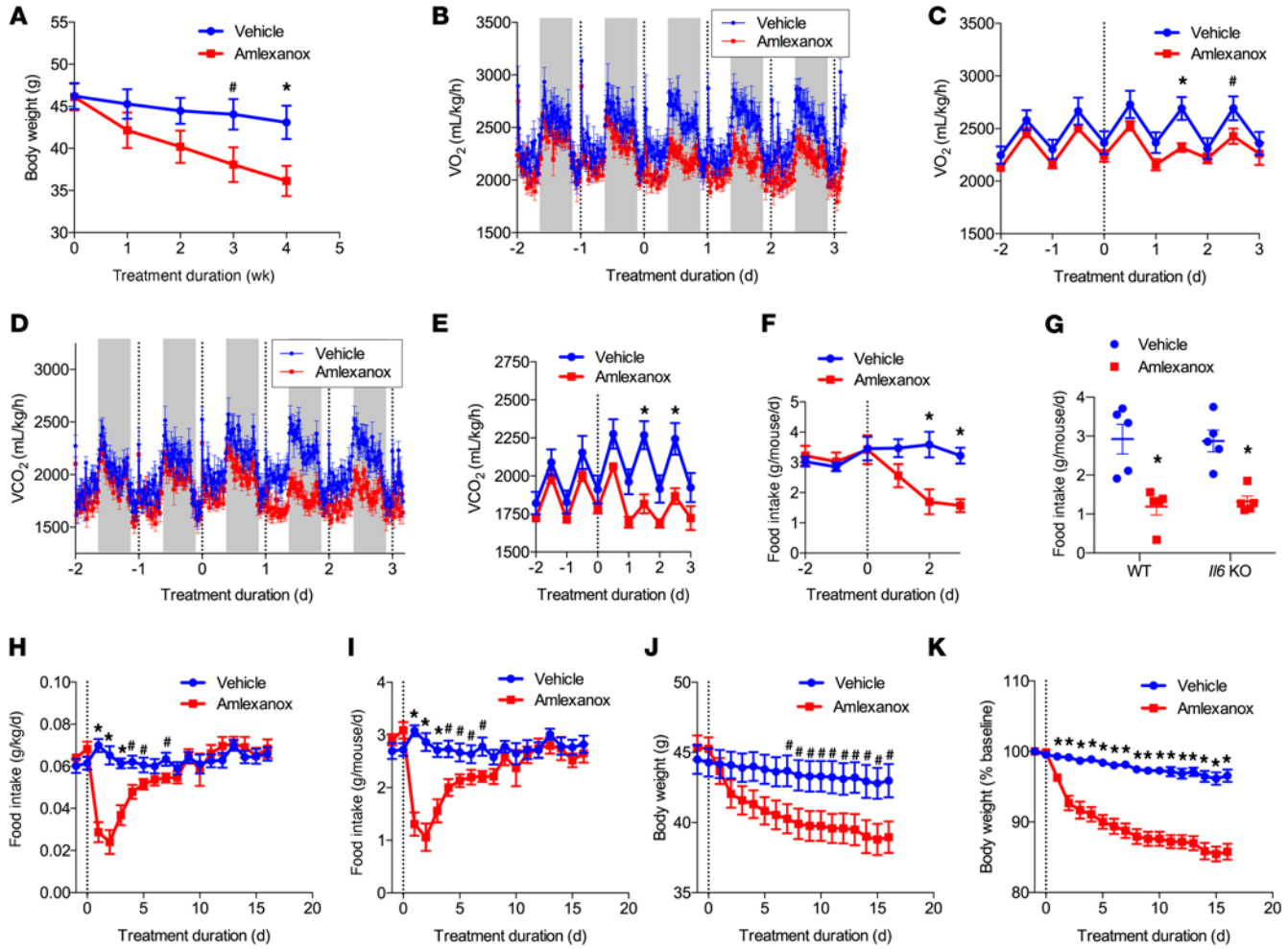

Figure 1. Amlexanox transiently reduces food intake. (**A**) Weekly body weights of obese mice treated with 25 mg/kg amlexanox or vehicle control. *n* = 7 vehicle-treated mice and *n* = 8 amlexanox-treated mice. (**B**–**F**) Metabolic cage experiment. *n* = 8 animals per treatment group. Vertical lines indicate treatment initiation and, in **B** and **D**, the time of daily treatment administration administration (day –1 vehicle control was administered to all). The dark cycle (6 pm to 6 am) is indicated in **B** and **D** by gray shading. (**B**) Oxygen consumption rate (VO_2). (**C**) Average oxygen consumption rate during the light or dark cycle. (**D**) Carbon dioxide production rate (VCO_2). (**E**) Average carbon dioxide production rate during the light or dark cycle. (**F**) Daily food intake. (**G**) Food intake 24–48 hours after treatment initiation for obese *Il6*-KO mice and littermate WT controls. WT versus *Il6*-KO values within treatment groups were not significantly different. *n* = 5 animals per genotype in each treatment group. (**H**–**K**) Daily food intake and body weights of obese mice treated with 25 mg/kg amlexanox or vehicle control. *n* = 9 vehicle-treated mice and *n* = 10 amlexanox-treated mice. (**H**) Body weight–normalized food intake. (**I**) Total food intake per mouse. (**J**) Body weight. (**K**) Body weight as a percentage of baseline body weight. $^*P < 0.05$, by Holm-Šídák post hoc test after significant 2-way ANOVA. $^\#P < 0.05$, by Student's *t* test, not corrected for multiple comparisons. Data are presented as the mean ± SEM.

animals exhibited significantly higher foraging activity than did the amlexanox-treated animals (Figure 2, B and C). We also observed higher x-ambulatory and total activity among the vehicle-treated mice during the first 2 dark cycles after treatment (Figure 2, D and E, and Supplemental Figure 3C). This increase in foraging activity in the vehicle-treated mice caused a spike in oxygen consumption and carbon dioxide production rates during the dark cycle on the first few days of treatment (Figure 2, F and G). Despite lower physical activity (Figure 2, B–E), the amlexanox-treated animals tended to have higher oxygen consumption and carbon dioxide production, a trend that reached statistical significance on the fourth day of treatment (Figure 2, H and I). By controlling for food intake, these data reveal that amlexanox treatment increased energy expenditure within the first few days of treatment. Although we did observe increased energy expenditure in the amlexanox-treated animals relative to pair-fed vehicle controls within the first week of treatment, the weight loss effect during this period was attributable to hypophagia, as we observed equal weight loss in the pair-fed vehicle controls (Figure 2J). Interestingly, weight loss in the amlexanox-treated animals was more concentrated in adipose tissue, as epididymal WAT (eWAT) and brown adipose tissue (BAT) weights relative to body weight were reduced in the amlexanox-treated mice versus the pair-fed, vehicle-treated mice (Figure 2K).

UCP1 and FGF21 are required for amlexanox-induced energy expenditure. Initial studies on amlexanox-induced weight loss revealed the activation of a thermogenic gene expression profile in WAT, leading us to hypothesize that the beiging of WAT promotes weight loss by increasing energy expenditure (21). To determine the contribution of adipocyte thermogenesis to weight loss in response to amlexanox, we treated obese *Ucp1*-KO and WT mice with amlexanox. We

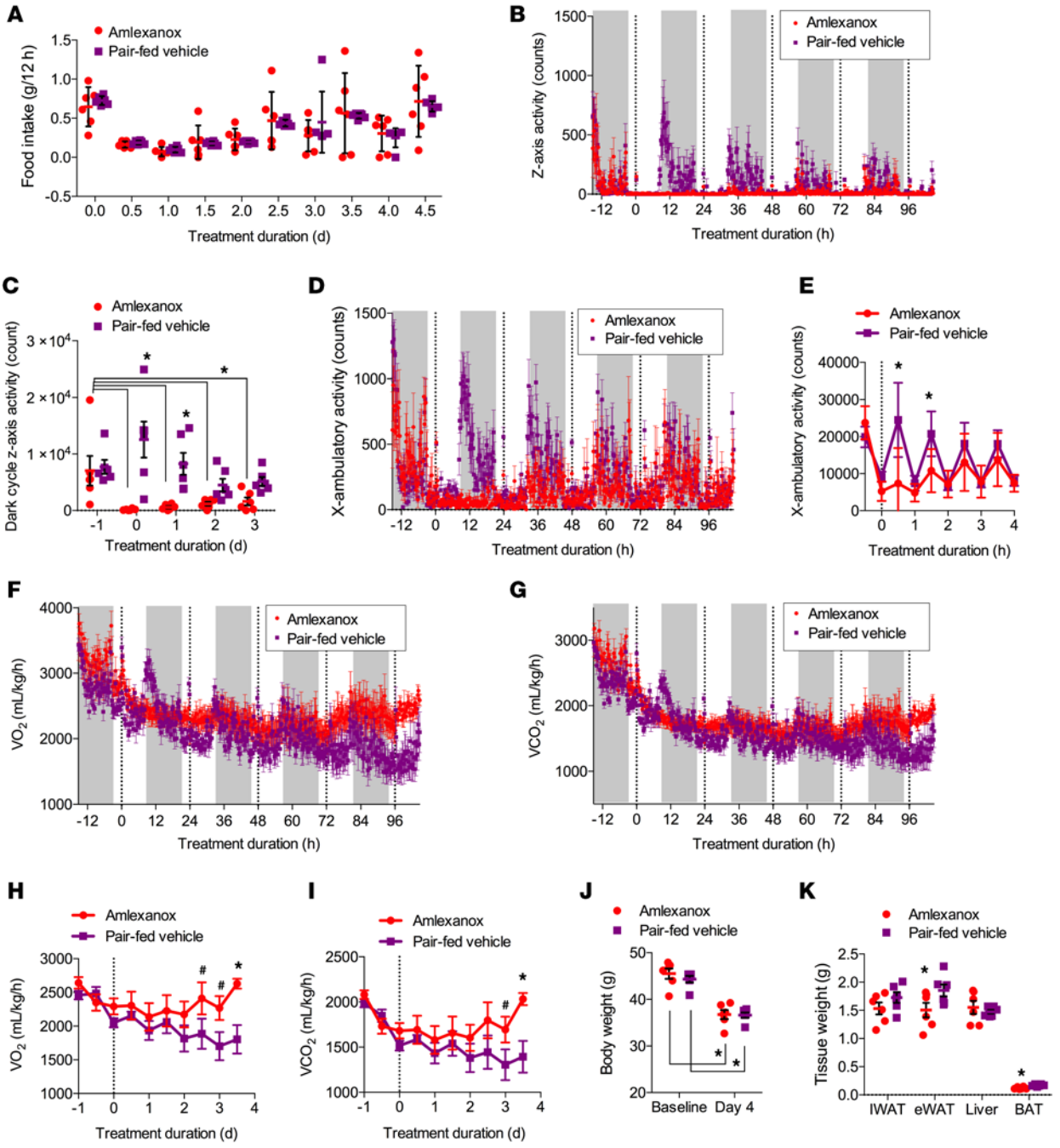

Figure 2. Amlexanox increases energy expenditure relative to pair-fed vehicle controls. Metabolic cage experiment in mice treated with amlexanox and pair-fed vehicle controls. Vertical lines indicate treatment administration. $n = 6$ animals per treatment group. (**A**) Food intake. (**B**) *Z*-axis activity. (**C**) Total *z*-axis activity during the dark cycle. (**D**) *X* axis ambulatory activity. (**E**) Total *x*-axis ambulatory activity during each light or dark cycle. (**F**) Oxygen consumption rate. (**G**) Carbon dioxide production rate. (**H**) Average oxygen consumption rate during the light or dark cycle. (**I**) Average carbon dioxide production rate during the light or dark cycle. (**J**) Body weights before and after the pair-fed metabolic cage experiment. (**K**) Tissue weights after the pair-fed metabolic cage experiment. $^{*}P < 0.05$, by Holm-Šidák post hoc test after significant 2-way ANOVA; $^{\#}P < 0.05$, by Student's *t* test, not corrected for multiple comparisons. Data are presented as the mean ± SEM.

found that initial weight loss was similar between genotypes (Figure 3A). After 2 weeks of treatment, weight loss was attenuated in the *Ucp1*-KO mice (Figure 3A). Thus, adipocyte thermogenesis via induction of UCP1 appears to be a critical component of amlexanox-induced energy expenditure and long-term weight loss. While the transient reduction in food intake promoted early weight loss in response to amlexanox, long-term weight loss was due to increased energy expenditure, mediated at least in part by the induction of UCP1 and the browning of WAT.

Next, we probed the mechanism of amlexanox-induced beiging of WAT. While investigating the effects of amlexanox on patients with obesity in a clinical trial, we observed a significant increase in the expression of *FGF21* mRNA in subcutaneous adipose tissue (26). Since FGF21 has been previously associated with

adipocyte thermogenesis (35, 36), we wondered whether FGF21 might play a role in amlexanox-induced energy expenditure. Thus, *Fgf21*-KO and WT littermate control mice were place on a HFD for 12 weeks and then treated with amlexanox or vehicle control. Similar to what we observed in the *Ucp1*-KO animals, *Fgf21*-KO mice exhibited a defect in amlexanox-induced weight loss after the first 2 weeks of treatment (Figure 3B), and the transient reduction in food intake was not affected by the absence of *Fgf21* (Figure 3C). Next, we assayed energy expenditure in a metabolic cage experiment between days 11 and 13 of amlexanox treatment, when the body weights of amlexanox-treated WT and *Fgf21*-KO mice began to diverge. Although amlexanox treatment in the WT animals was associated with a substantial increase in energy expenditure, this effect was absent in *Fgf21*-KO mice (Figure 3, D and E). This defect in energy expenditure was associated with an attenuated induction of *Ucp1* and *Dio2* gene expression in inguinal WAT (iWAT) by amlexanox in the *Fgf21*-KO animals (Figure 3, F and G). Consistent with increased energy expenditure and reduced adiposity, WT mice treated with amlexanox had reduced lipid droplet size in both WAT (iWAT and eWAT) and BAT (Figure 3H). *Fgf21*-KO mice did not exhibit a reduction in lipid droplet size upon amlexanox treatment (Figure 3H and Supplemental Figure 4). Taken together, these data indicate that FGF21 is required for the induction of thermogenic gene expression and increased energy expenditure that mediate long-term weight loss in response to amlexanox.

Weight loss in response to surgery (gastric bypass) and caloric restriction are associated with browning of WAT (37, 38), suggesting beiging of WAT is commonly associated with a negative energy balance. To determine whether the FGF21-dependent browning of WAT occurs independently of weight loss, we treated nonobese WT and *Fgf21*-KO mice with amlexanox. The beiging of WAT was readily observable by immunohistochemistry staining for UCP1 in the iWAT of WT animals treated with amlexanox for just 1 week; however, this effect was greatly reduced in the *Fgf21*-KO animals (Supplemental Figure 5A). Furthermore, while *Ucp1* and *Dio2* expression was higher in the amlexanox–treated WT mice relative to vehicle controls, we observed no significant increase in the *Fgf21*-KO mice after amlexanox treatment (Supplemental Figure 5, B and C). As previously observed, normal diet–fed (ND-fed) mice did not show reductions in weight or food intake in response to amlexanox (Supplemental Figure 5, D–F). Thus, we can conclude that FGF21-induced browning of WAT is probably the cause and not the consequence of weight loss in the obese mice.

Amlexanox treatment promotes thermogenesis. Next we investigated whether the beiging of WAT in response to amlexanox affected thermogenesis. To dissect the effect of amlexanox versus food intake on thermoregulation, we compared changes in the core body temperature of amlexanox-treated animals with that of both pair-fed and ad libitum–fed vehicle control mice. Consistent with previous experiments, amlexanox treatment caused transient hypophagia, which was greatest in the first week of treatment (Figure 4A). This acute hypophagia dictated weight loss in the first week of treatment, which was equal between the amlexanox-treated and pair-fed vehicle controls (Figure 4B). Interestingly, although the pair-fed vehicle control mice exhibited the expected hypothermic response to hypophagia (39–41), the amlexanox-treated animals had increased core body temperatures during this period (Figure 4C). In the third and fourth weeks of treatment, when food intake had returned to normal, the pair-fed vehicle controls began to regain weight, and their core temperature returned to baseline (Figure 4, A–C). Meanwhile, the amlexanox-treated mice maintained their weight loss and continued to lose weight (Figure 4B). Consistent with a thermogenic mechanism of weight loss, the amlexanox-treated animals had higher core body temperatures in the third and fourth weeks of treatment (Figure 4C). Although both amlexanox-treated and pair-fed vehicle control mice exhibited a reduction in adiposity, this effect was greater in the amlexanox-treated animals (Figure 4D). The increase in core body temperature in the amlexanox-treated mice was not observed in *Fgf21*-KO mice, indicating that this effect was FGF21 dependent (Figure 4E).

Hepatic FGF21 secretion is responsible for circulating FGF21, but is dispensable for beiging in response to amlexanox. It has previously been observed that hepatic FGF21 secretion is increased in the fasted state to regulate systemic metabolism (42–45). Administration of amlexanox by oral gavage elevated serum FGF21, reaching maximal levels after 24 hours (Figure 5A). We observed an increase in *Fgf21* mRNA expression in iWAT and BAT, but not liver, 4 hours after amlexanox treatment (Figure 5B). However, liver *Fgf21* expression increased after 24 hours (Figure 5C). Because fasting induces hepatic FGF21 secretion, it is possible that food restriction induced by amlexanox promotes hepatic FGF21 secretion. Since we observed an early increase in *Fgf21* expression in adipose tissue, and later in the liver, we used liver-specific *Fgf21*-KO mice (FLKO) to determine the relative importance of hepatic *Fgf21* to circulating FGF21 and the FGF21-dependent phenotypes produced by amlexanox treatment (Figure 5, D–G). Consistent with prior work demonstrating that circulating FGF21 is derived from the liver (43), we found that serum FGF21 levels were low in the FLKO mice and did not increase with 24-hour amlexanox treatment (Figure 5D). This effect was specific to FGF21, as serum IL-6 levels increased normally in response to amlexanox treatment in the FLKO animals (Figure 5E). Surprisingly, there was no defect in weight loss in the FLKO mice (Figure 5F), contrary to what we observed in the whole-body *Fgf21*–KO animals (Figure 3B). In accordance with equal weight loss, hyperinsulinemia was reduced equally in WT and FLKO mice by amlexanox treatment (Figure 5G). Furthermore, WT and FLKO mice showed similar levels of *Ucp1* and *Dio2* expression in their WAT in response to amlexanox (Figure 5, H and I). These data indicate that hepatic secretion of FGF21 into the serum is dispensable for amlexanox-induced WAT beiging and subsequent weight loss and that the defect in the whole-body KO mice must have been due to another pool of FGF21.

Amlexanox stimulates adipocyte FGF21 secretion. Although liver-specific KO of *Fgf21* ablated the increase in circulating FGF21, we detected no change in the responsiveness of these mice to amlexanox (Figure 5, F–I). This led us to wonder whether FGF21 secreted from adipocytes might act locally to promote thermogenic gene expression and energy expenditure, as observed in the exocrine pancreas (46). First, we investigated FGF21 expression and secretion in adipocytes. For these experiments, we used primary preadipocytes (isolated from iWAT) differentiated in vitro (PPDIVs). Amlexanox treatment robustly stimulated *Fgf21* expression (Figure 6A) as well as FGF21 protein secretion into the media (Figure 6B).

We have previously shown that IKKε inhibits cAMP signaling by activating PDE-3, and that inhibition of IKKε with amlexanox

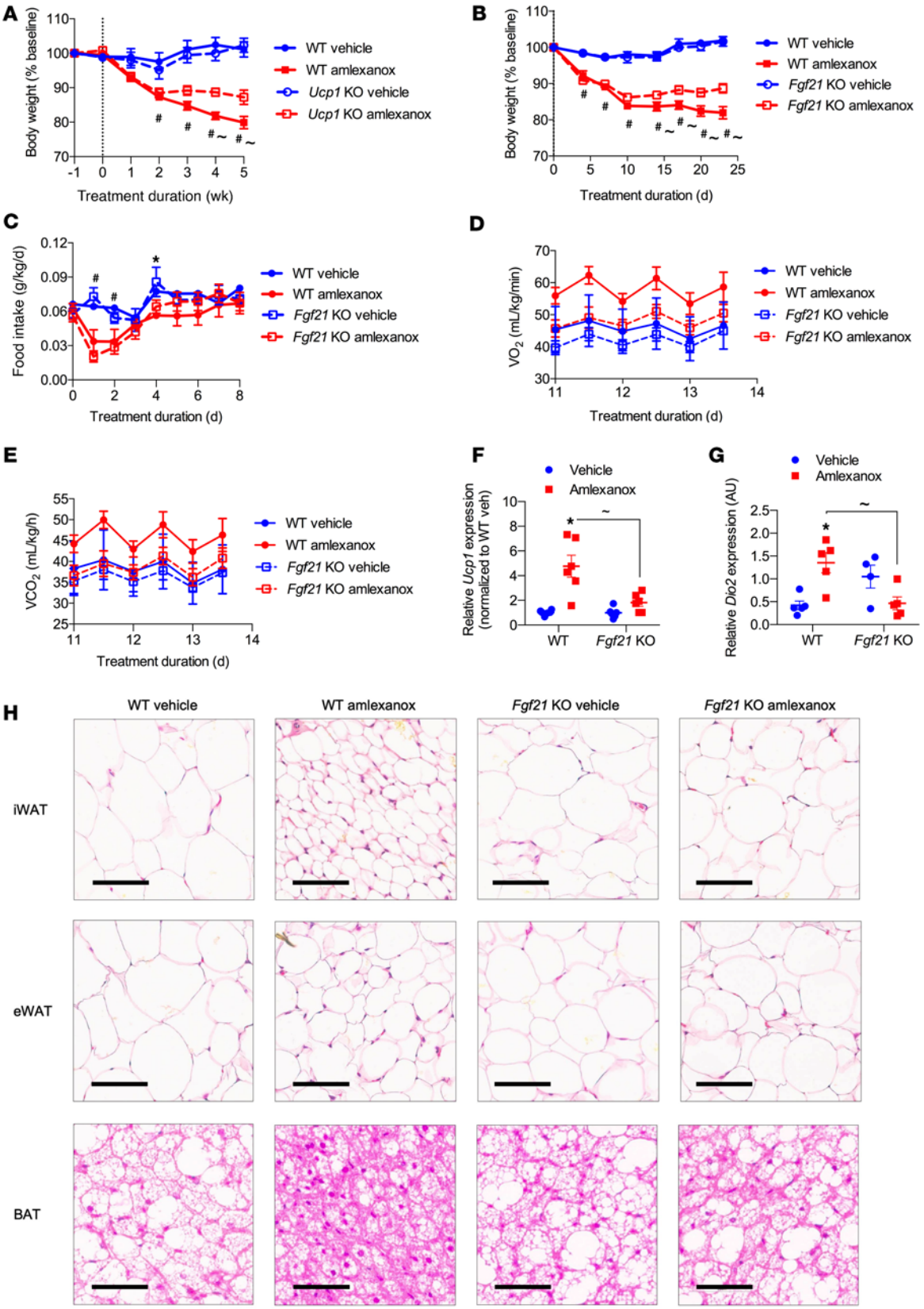
A
Body weight (% baseline)
Treatment duration (wk)
WT vehicle
WT amlexanox
Ucp1 KO vehicle
Ucp1 KO amlexanox
B
Body weight (% baseline)
Treatment duration (d)
WT vehicle
WT amlexanox
Fgf21 KO vehicle
Fgf21 KO amlexanox
C
Food intake (g/kg/d)
Treatment duration (d)
WT vehicle
WT amlexanox
Fgf21 KO vehicle
Fgf21 KO amlexanox
D
VO2 (mL/kg/min)
Treatment duration (d)
WT vehicle
WT amlexanox
Fgf21 KO vehicle
Fgf21 KO amlexanox
E
VCO2 (mL/kg/h)
Treatment duration (d)
WT vehicle
WT amlexanox
Fgf21 KO vehicle
Fgf21 KO amlexanox
F
Relative Ucp1 expression (normalized to WT veh)
Vehicle
Amlexanox
WT
Fgf21 KO
G
Relative Dio2 expression (AU)
Vehicle
Amlexanox
WT
Fgf21 KO
H
WT vehicle
WT amlexanox
Fgf21 KO vehicle
Fgf21 KO amlexanox
iWAT
eWAT
BAT

Figure 3. FGF21 is required for adipose tissue beiging and weight loss in response to amlexanox. (**A**) Weekly body weights of obese *Ucp1*-KO mice and WT littermates treated with 25 mg/kg amlexanox by daily oral gavage, expressed as a percentage of baseline body weight. n = 6 animals per genotype in each treatment group. (**B**–**H**) Obese *Fgf21*-KO and WT littermates were treated with 25 mg/kg amlexanox by daily oral gavage. (**B**) Body weight expressed as a percentage of baseline body weight. n = 5 WT and 6 KO animals per treatment group. (**C**) Body weight–normalized food intake for the mice in **B**. (**D**) Oxygen consumption and (**E**) carbon dioxide production rates measured by metabolic cages for the mice in **B**, starting on day 11 of treatment. (**F**) *Ucp1* expression in iWAT after 4 weeks of treatment. n = 6 animals per genotype in each treatment group. veh, vehicle. (**G**) *Dio2* expression in iWAT after 4 weeks of treatment. n = 5 animals per genotype in each treatment group. (**H**) Representative H&E-stained sections after 4 weeks of treatment. Scale bars: 100 μm (iWAT), 100 μm (eWAT), and 50 μm (BAT). Statistical significance was determined by Holm-Šidák post hoc test after significant 2-way ANOVA. $^{*}P < 0.05$ for vehicle versus amlexanox treatment. $^{\#}P < 0.05$ for vehicle versus amlexanox in both WT and KO mice. $^{-}P < 0.05$ for WT versus KO mice in the amlexanox-treated group. Data are presented as the mean ± SEM.

restores cAMP signaling and a cAMP transcriptional program that is dependent on the activation of p38 MAPK (29). Adipocyte FGF21 expression has previously been linked to sympathetic activation of adipocyte cAMP signaling (35, 47, 48). To determine whether FGF21 expression is mediated via this pathway, we pretreated PPDIVs with the specific p38 inhibitor SB-203,580, which completely blocked the induction of *Fgf21* gene expression and FGF21 protein secretion into the media (Figure 6, A and B). We also examined the effect of p38 inhibition in vivo by pretreating mice with 20 mg/kg SB-203,580 before a 4-hour amlexanox treatment. Hepatic *Fgf21* was not induced at this time point (Figure 5B), and serum FGF21 levels were not elevated (Figure 5A). Accordingly, neither amlexanox nor SB-203,580 treatment impacted serum FGF21 levels (Figure 6C). Pretreatment of mice with SB-203,580 in vivo blocked the amlexanox-dependent induction of *Fgf21* expression in WAT (Figure 6D). Interestingly, SB-203,580 treatment also prevented the induction of *Ucp1* expression in WAT (Figure 6E).

To determine whether amlexanox-induced *Ucp1* expression could be mediated by autocrine FGF21 action, we treated WT and *Fgf21*-KO PPDIVs with amlexanox. As expected, amlexanox treatment induced *Fgf21* expression in the WT PPDIVs, whereas *Fgf21* expression was not detectable in the *Fgf21*-KO cells (Figure 6F). The induction of *Il6* and *Atf3* expression by amlexanox was equal in both genotypes (Figure 6, G and H). Conversely, although amlexanox treatment induced *Ucp1* expression in WT PPDIVs, this effect was notably absent in *Fgf21*-KO PPDIVs (Figure 6I), indicating that adipocyte-derived FGF21 could function as a local autocrine factor that plays a key role in the induction of *Ucp1* expression in response to amlexanox. We found that the induction of *Dio2* expression by amlexanox was similarly dependent on FGF21 (Figure 6J), indicating a generalized defect in browning. WAT browning in vivo occurs both by increased expression of thermogenic genes in mature adipocytes and increased differentiation of beige adipocytes, which requires 1 week or more. Amlexanox appeared to induce *Ucp1* expression via both mechanisms, as *Ucp1* expression was acutely elevated and increased further after more than 1 week of treatment (Supplemental Figure 6A). While *Fgf21* expression in iWAT was only elevated acutely (Supplemental Figure 6B), it was required for the initiation of beiging (Figure 5, F–I), which then led to increased energy expenditure and subsequent weight loss. Thus the FGF21-dependent weight loss produced by amlexanox (Figure 3, A and B) lagged behind the induction of FGF21 itself.

Adipocyte-secreted FGF21 is required for amlexanox-induced energy expenditure. These results led us to predict that adipocyte-specific KO of *Fgf21* (FAKO) would cause a defect in the beiging of adipose tissue in response to amlexanox without affecting circulating FGF21 levels. Indeed, the increase of circulating FGF21 levels produced in response to amlexanox was equal in WT and FAKO littermate animals (Figure 7A). Nevertheless, the expression of *Ucp1* and *Dio2* was significantly attenuated in FAKO mice compared with expression in WT controls after just 8 days of amlexanox treatment (Figure 7, B and C). Importantly, inhibition of thermogenic gene expression in the FAKO animals corresponded to an attenuation of amlexanox-induced weight loss (Figure 7D). These data suggest that FGF21 secreted by adipocytes acts locally to promote beiging and thermogenic gene expression with amlexanox treatment. Consistent with this idea, protein levels of FGF21 in the adipose tissue after amlexanox treatment were comparable to protein levels found in the liver (Figure 7, E and F, and Supplemental Figure 7, A and B). Furthermore, the increase in adipose tissue FGF21 levels in FLKO mice was similar to that observed in WT mice (Figure 7, G and H, and Supplemental Figure 7C).

Regulation of insulin sensitivity and glucose handling by amlexanox. Although the reductions in food intake were transient and contributed only to initial weight loss, we wondered whether they might play a role in the reduction of fasting blood glucose levels observed on the third day of amlexanox treatment (29). We previously proposed that acute reductions in fasting blood glucose produced by amlexanox are mediated by a subcutaneous adipose tissue-to-liver axis, whereby adipocyte-secreted IL-6 activates hepatic STAT3 to suppress hepatic glucose production (29). To differentiate this axis from the effects of reduced food intake, we examined fasting blood glucose levels in *Il6*-KO mice, which do not exhibit a defect in suppression of food intake in response to amlexanox treatment (Figure 1G). Despite equal reductions in food intake in the *Il6*-KO and WT animals, fasting blood glucose levels were suppressed in the WT animals, but not in the *Il6*-KO mice treated with amlexanox (Figure 8A). To further investigate this signaling axis, we generated mice with liver-specific KO of *Stat3* (SLKO) by crossing albumin-Cre (*Alb-Cre*) mice with *Stat3*-floxed mice. STAT3 protein levels were markedly reduced in the SLKO liver lysates (Supplemental Figure 8, A and B). Treatment of WT mice with amlexanox produced robust STAT3 tyrosine 705 phosphorylation in liver (Supplemental Figure 8A). We detected only a small amount of residual STAT3 in the SLKO livers, probably from the nonhepatocytes.

Weight loss in the SLKO and WT mice was equal after 3 days of amlexanox treatment (Figure 8B), indicating that, like KO of *Il6*, hepatic STAT3 deficiency does not affect amlexanox-induced hypophagia. Thus, the relative effect of the adipose-to-liver axis versus food intake on reductions in fasting blood glucose observed with acute amlexanox treatment can be specifically evaluated using SLKO animals. Although fasting blood glucose levels were significantly lower in amlexanox-treated mice relative to vehicle-treated WT littermate controls, this difference was not observed in the

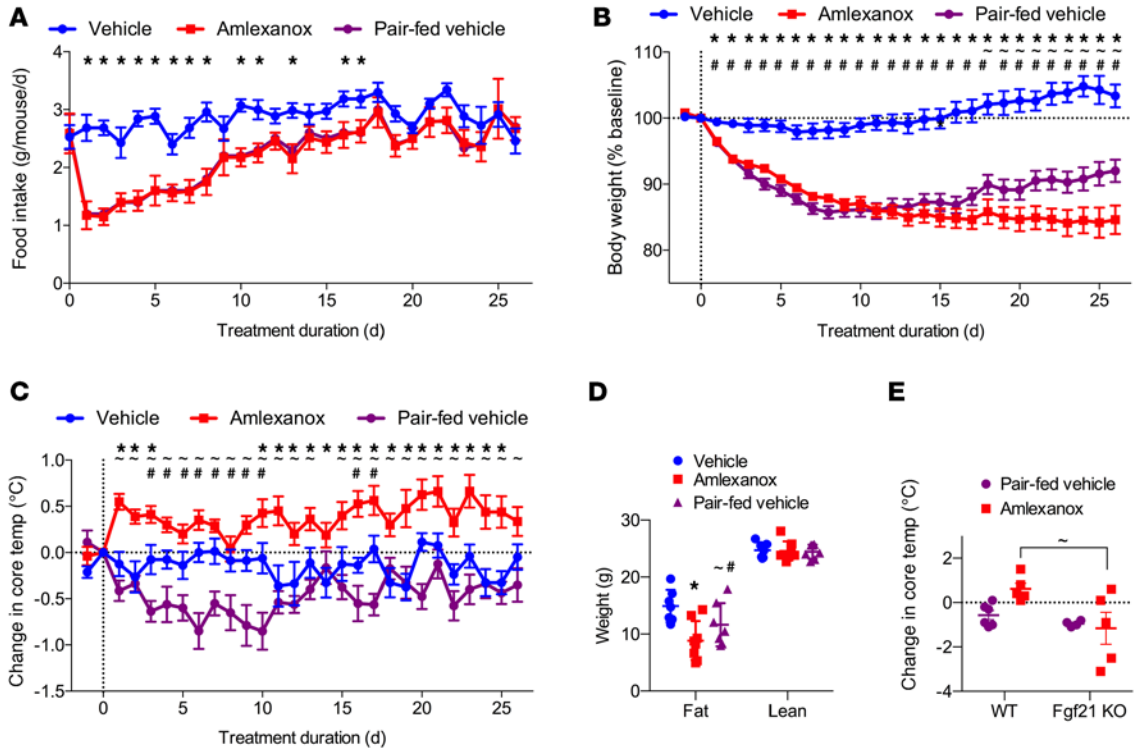

Figure 4. Amlexanox increases thermogenesis. (**A**–**D**) Obese mice were treated with 25 mg/kg amlexanox or vehicle control daily. Amlexanox- and vehicle-treated animals were fed ad libitum, whereas pair-fed, vehicle-treated animals were provided the averaged amount of food consumed by the amlexanox-treated group. n = 6–7 mice per treatment group. (**A**) Food intake, (**B**) body weight, and (**C**) rectal temperatures (temp) were measured daily 5 hours into the light cycle, just before daily treatment administration. (**D**) Total fat and lean mass measured by MRI after 26 days of treatment. (**E**) Rectal temperatures of obese WT and *Fgf21*-KO mice treated with 25 mg/kg amlexanox and of pair-fed, vehicle-treated controls after 24 hours of treatment. Statistical significance was determined by Holm-Šidák post hoc test after significant 2-way ANOVA. $^{*}P < 0.05$ for vehicle- versus amlexanox-treated mice. $^{\sim}P < 0.05$ for amlexanox- versus pair-fed, vehicle-treated mice (**A**–**D**) and WT versus KO mice in the amlexanox-treated group (**E**). $^{\#}P < 0.05$ for vehicle- versus pair-fed, vehicle-treated groups. Data are presented as the mean ± SEM.

SLKO animals (Figure 8C). Amlexanox increased hepatic expression of *Socs3*, a STAT3 target gene (49–51), reflecting hepatic STAT3 transcriptional regulation (Figure 8D). This response was absent in the SLKO animals (Figure 8D). Hepatic STAT3 suppresses glucose production via a reduction of *G6pc* expression (52–54). Accordingly, we observed suppression of *G6pc* expression in the WT animals treated with amlexanox (Figure 8E). However, we detected no suppression of *G6pc* expression in response to amlexanox in the SLKO animals (Figure 8E). The suppression of hepatic glucose production by amlexanox was apparent in the lower blood glucose levels during a pyruvate tolerance test (Figure 8F). This effect of amlexanox was notably absent in the SLKO animals, demonstrating that hepatic STAT3 is required for the suppression of hepatic glucose production by amlexanox (Figure 8F).

We also examined the role of adipocyte FGF21 in reducing fasting blood glucose levels in response to amlexanox treatment. Although the FAKO mice exhibited defects in weight loss in response to amlexanox, fasting blood glucose levels were reduced equally in the FAKO and WT animals (Figure 8G). These results indicate that, while a reduction in food intake contributes to initial weight loss during amlexanox treatment, it is not the driving factor in reducing fasting blood glucose, which is instead mediated by the activation of hepatic STAT3 by IL-6 and a subsequent suppression of hepatic gluconeogenesis.

Next, we turned our attention to the improvements in insulin sensitivity observed in response to amlexanox treatment. The reduction in fasting blood glucose did not translate to improved insulin sensitivity. The suppression of hepatic glucose production by amlexanox resulted in lower glucose levels in WT mice throughout an insulin tolerance test (Supplemental Figure 8C). While *Il6*-KO mice did not exhibit this overall reduction in fasting blood glucose, baseline normalization revealed that both WT and *Il6*-KO mice had the same degree of insulin sensitization after amlexanox treatment (Supplemental Figure 8, C and D). Accordingly, the ability of amlexanox to improve insulin sensitivity was identical in SLKO mice and their WT floxed littermates (Figure 8H). Moreover, SLKO mice exhibited normal weight loss in response to 4 weeks of amlexanox treatment (Figure 8I). Thus, the weight loss and insulin sensitization produced by amlexanox were not dependent on the IL-6/STAT3 pathway that acutely suppressed hepatic glucose production.

Given the correlation between body weight and insulin sensitivity, it is possible that the improvements in insulin sensitivity were secondary to amlexanox-induced weight loss. Thus, we assessed insulin sensitivity in *Fgf21*- and *Ucp1*-KO animals, which exhibit defects in weight loss. Indeed, the reduction of fasting insulin levels by amlexanox was attenuated in both *Fgf21*- and *Ucp1*-KO animals (Figure 8, J and K). Furthermore, although WT animals showed significant insulin sensitization in an insulin tolerance test after 4 weeks amlexanox

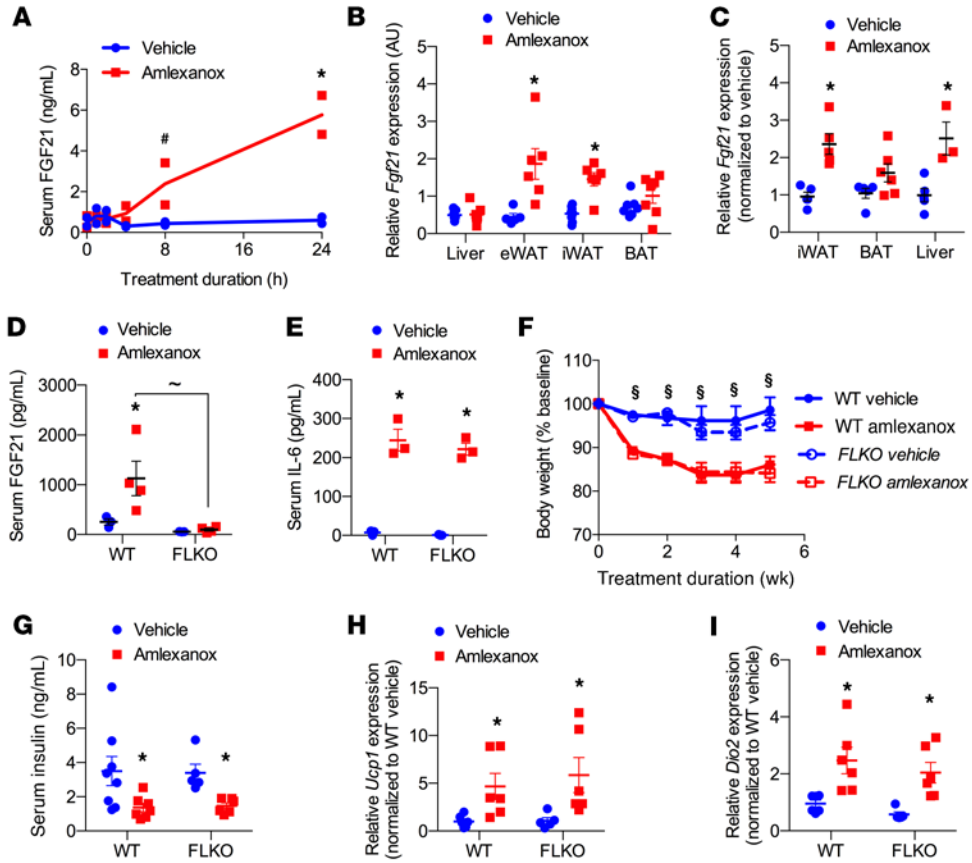

Figure 5. Hepatic FGF21 secretion determines circulating FGF21 levels but not beiging of WAT. (**A**) Serum FGF21 levels after treatment with 25 mg/kg amlexanox or vehicle control. n = 2 animals per treatment per time point. (**B** and **C**) Amlexanox induced *Fgf21* expression in various tissues relative to vehicle control treatment. (**B**) *Fgf21* expression after 4 hours of treatment. n = 7 animals per treatment group. (**C**) *Fgf21* expression after 24 hours of treatment. n = 5 animals per treatment. (**D**–**I**) FLKO and WT littermate control animals were treated with 25 mg/kg amlexanox or vehicle. (**D**) Serum FGF21 levels after 24 hours of treatment. n = 3 vehicle-treated and n = 4 amlexanox-treated animals per genotype. (**E**) Serum IL-6 levels after 24 hours of treatment. n = 3 animals per genotype per treatment. (**F**) Weight as a percentage of baseline body weight. n = 8 WT and n = 6 FLKO animals per treatment. (**G**) Serum insulin levels after 4 weeks of treatment. n = 8 WT and n = 6 FLKO animals per treatment. Expression of (**H**) *Ucp1* and (**I**) *Dio2* in eWAT tissue after 5 weeks of treatment. n = 6 animals per genotype per treatment. $^{*}P < 0.05$, by Holm-Šidák post hoc test after significant 2-way ANOVA for the vehicle- versus amlexanox-treated groups. $^{\S}P < 0.05$, by Holm-Šidák post hoc test after significant 2-way ANOVA for the vehicle- versus amlexanox-treated in both WT and KO groups. $^{\sim}P < 0.05$ for WT versus KO animals in the amlexanox-treated group. $^{\#}P < 0.05$, by Student's t test, not corrected for multiple comparisons. Data are presented as the mean ± SEM.

treatment, we did not observe amlexanox-induced insulin sensitization in either *Fgf21*-KO or *Ucp1*-KO animals (Figure 8, L and M). These results suggest that the insulin-sensitizing effects of amlexanox were secondary to increased energy expenditure.

Discussion

Current approaches to obesity are only marginally effective, and new therapies are needed (55). Numerous studies have shown that obesity is associated with chronic low-grade inflammation in both dietary and genetic rodent models, as well as in humans, and further that this inflammation is associated with insulin resistance and decreased energy expenditure (8, 9, 15–17). Obesity induces increased infiltration of inflammatory cells into liver and adipose tissue as well as increases in inflammatory pathways in fat and liver cells (8, 9, 13, 14, 56, 57). Among the changes is activation of the NF-κB pathway, which is associated with increased expression and activity of the noncanonical Iκβ kinases IKKε and TBK1. These findings led us to search for inhibitors of these kinases, and we discovered that the asthma drug amlexanox was a selective dual-specificity inhibitor that reverses many of the effects of HFD-induced and genetically induced obesity in both rodents (21) and humans (26). Here, we report that treatment of mice with amlexanox produced a coordinated crosstalk between adipose tissue and liver involving a network of endocrine and autocrine factors that together increased energy expenditure and reduced glycemia, resulting in weight loss and improved insulin sensitivity.

We followed the effects of amlexanox on energy metabolism in obese mice over the first days of treatment and, surprisingly, discovered a transient reduction in food intake that contributed to early weight loss in response to the drug. Interestingly, this effect was observed only in animals with preexisting obesity. It has previously been shown that hypothalamic IKKε levels are elevated in obese mice as a consequence of increased inflammation and contribute to central leptin resistance (58–60). Furthermore, inhibition or knockdown of IKKε in the brain caused acute reductions in food intake (58). Thus, amlexanox may suppress food intake via direct inhibition of hypothalamic IKKε. While we hypothesize that this transient hypophagia is the result of a central effect on satiety, illness-like behavior cannot be definitively ruled out. Much additional work is required to tease apart

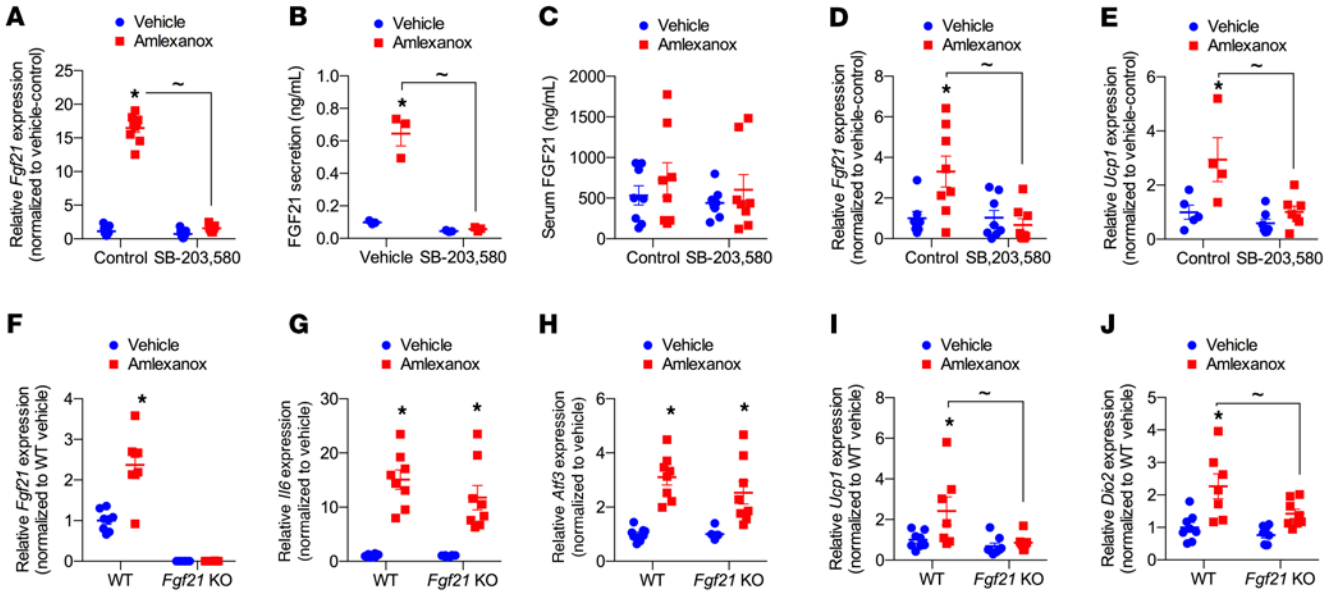

Figure 6. Adipocyte-secreted FGF21 promotes adipocyte *Ucp1* expression. (**A** and **B**) PPDIVs were treated with 1 mg/mL SB-203,850 or control for 30 minutes before vehicle or 100 μM amlexanox treatment. (**A**) *Fgf21* expression after a 2-hour treatment. *n* = 9 wells per condition. (**B**) FGF21 secretion into the media after a 4-hour treatment. *n* = 3 wells per condition. (**C**–**E**) Obese mice were pretreated with 20 mg/kg SB-203,850 or control for 30 minutes before treatment with vehicle or 25 mg/kg amlexanox for 4 hours. *n* = 8 mice per treatment condition. (**C**) FGF21 serum levels. (**D**) *Fgf21* expression in iWAT. (**E**) *Ucp1* expression in iWAT. Expression of (**F**) *Fgf21*, (**G**) *Il6*, (**H**) *Atf3*, (**I**) *Ucp1*, and (**J**) *Dio2* in *Fgf21*-KO and WT control PPDIVs treated with vehicle or 100 μM amlexanox for 4 hours. $^{*}P < 0.05$, by Holm-Šidák post hoc test after significant 2-way ANOVA for vehicle versus amlexanox treatment. $^{\sim}P < 0.05$ for WT versus KO or control versus SB-203,850 in the amlexanox-treated group. Data are presented as the mean ± SEM.

the central and peripheral effects of amlexanox on feeding behavior, and the underlying molecular mechanisms, and to determine whether this effect occurs in humans.

Although this acute reduction in food intake coincided with a reduction in fasting blood glucose, these 2 events appeared to be distinct and not causally related. The reduction in fasting blood glucose resulted from suppression of hepatic glucose production due to the activation of hepatic STAT3 by adipocyte-secreted IL-6, since the reduction in hepatic glucose production and fasting blood glucose was not observed in *Il6*-KO (29) or liver-specific *Stat3*-KO mice treated with amlexanox, whereas both mouse models exhibited the same transient reduction in food intake and early weight loss in response to amlexanox observed in WT animals. Interestingly, the suppression of hepatic glucose production and fasting blood glucose was also mechanistically distinct from its effects on insulin sensitivity. Improved insulin sensitivity correlated with the beiging of WAT and weight loss.

While the effect of amlexanox on food intake was transient, weight loss persisted beyond the first days of treatment with the drug, presumably because of the increased thermogenic energy expenditure. Amlexanox treatment blocked the hypothermic response to reduced caloric intake and further increased thermogenesis. This was accompanied by increased browning or beiging of subcutaneous WAT, along with the increased expression of thermogenic genes such as *Ucp1* and others. This finding was consistent with the increases in catecholamine sensitivity observed with inhibition or KO of IKKε in adipocytes (27, 28) and suggests that increased cAMP signaling in adipocytes is responsible for elevated energy expenditure. Of note, although UCP1 expression correlates with adipose tissue beiging and energy expenditure, mitochondrial defects in UCP1-KO mice (61) preclude the exclusion of UCP1-independent changes in mitochondrial bioenergetics that may also contribute to energy expenditure.

What is the mechanism of the amlexanox-induced increase in energy expenditure? In a randomized, placebo-controlled clinical trial of amlexanox in patients with obesity and type 2 diabetes, we obtained biopsies of treated patients and extracted RNA to measure changes in gene expression (26). These studies revealed increased expression of the *FGF21* gene in response to amlexanox that correlated well with effectiveness of the drug, leading us to measure FGF21 protein levels and gene expression in obese mice treated with amlexanox. We observed a dramatic increase in *Fgf21* mRNA in liver and adipose depots, as well as an increase in circulating levels of the hormone in response to treatment with the drug. Moreover, global FGF21–KO mice were refractory to the beneficial metabolic effects of amlexanox, indicating that expression of this hormone is crucial for the actions of the drug.

Interestingly, the increased expression of hepatic *Fgf21* mRNA and its secretion into the circulation in response to amlexanox appeared to be dispensable for weight loss, whereas the local secretion and action of FGF21 in WAT appeared to be critical for adipose tissue browning. Circulating FGF21 levels were negligible in FLKO mice, yet these animals still exhibited WAT browning in response to amlexanox treatment, an effect notably absent in *Fgf21* whole-body–KO mice, suggesting that another pool of FGF21 affected adipocyte function, without impacting circulating FGF21 levels. We thus propose that adipocytes are mainly responsive to locally produced FGF21. Indeed, FAKO mice showed no reduction in serum FGF21 levels, but did not exhibit browning of WAT in response to amlexanox treatment. FAKO mice also showed a defect in weight

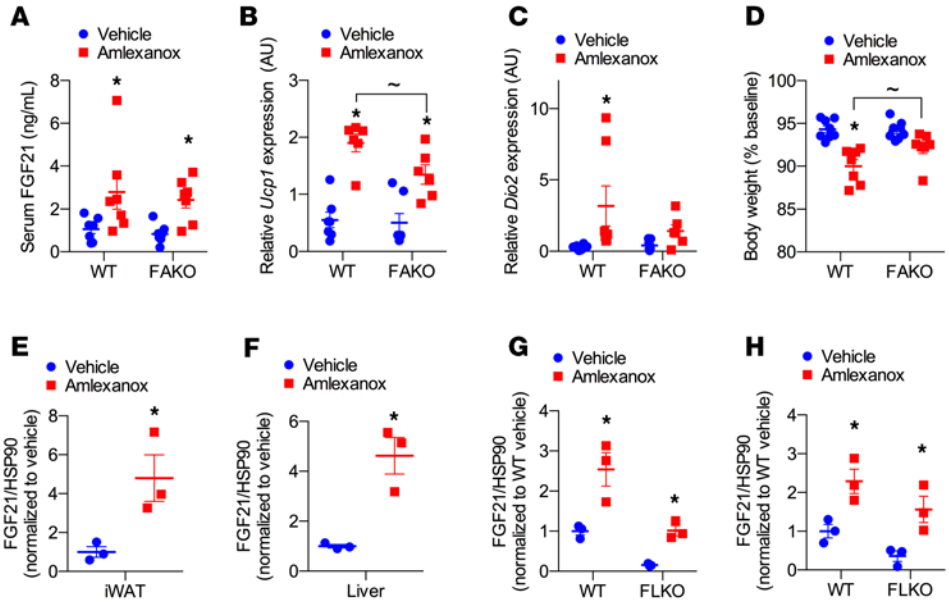

Figure 7. Effects of amlexanox in adipose- and liver-specific *Fgf21*–KO mice. (**A**–**D**) Obese FAKO and WT littermate control animals were treated with 25 mg/kg amlexanox or vehicle. n = 8 vehicle- and n = 7 amlexanox-treated animals per genotype. (**A**) Serum FGF21 levels. (**B**) *Ucp1* expression in iWAT. (**C**) *Dio2* expression in iWAT. (**D**) Weight loss, presented as a percentage of baseline body weight. (**E**–**H**) Quantification of FGF21 protein levels normalized to HSP90 protein detected by Western blotting 24 hours after treatment (see also Supplemental Figure 4). (**E**) FGF21 levels in WT iWAT. (**F**) FGF21 levels in WT liver. (**G**) FGF21 levels in WT and FLKO iWAT. (**H**) FGF21 levels in WT and FLKO eWAT. n = 3 animals per treatment per genotype. *$P < 0.05$, by Holm-Šidák post hoc test after significant 2-way ANOVA for the vehicle- versus amlexanox-treated groups. $^{-}P < 0.05$ for WT versus KO animals in the amlexanox-treated group. Data are presented as the mean ± SEM

loss after only 8 days of treatment. Long-term experiments would be expected to demonstrate a greater defect in weight loss. Taken together, these results strongly indicate that adipocyte-secreted FGF21 acts locally to promote the browning of WAT, but does not enter the circulation. Thus, FGF21 behaves as an autocrine factor in adipocytes in response to amlexanox administration.

The core body temperature of the mice was increased by amlexanox treatment, both acutely after the first day of treatment and after 2 weeks of daily treatment. WAT beiging at least partly required the differentiation of beige adipocytes and was thus consistent with the increase in thermogenesis after 2 weeks of treatment. However, beiging was unlikely to account for the early transient increase in thermogenesis, which was more likely the result of central FGF21 action promoting BAT thermogenesis via sympathetic activation. Although the long-term thermogenic effect of amlexanox was associated with weight loss, the acute effect was not observed to significantly affect body weight, probably because of its transient nature.

FGF21 has emerged as a therapeutic agent to treat obesity and associated metabolic disorders. While exogenous administration of FGF21 and its analogs has shown beneficial metabolic effects, our understanding of its role in the control of energy homeostasis remains incomplete (62–65). Although our data suggest that adipose tissue is a critical target tissue for FGF21 action, whether exogenous FGF21 can effectively control adipocyte metabolism when delivered at reasonable doses remains uncertain. Unlike other members of the FGF family, FGF21 does not bind to heparin sulfate, which makes the protein relatively soluble and permits secretion from hepatocytes into the circulation (66). Sequestration of FGF21 in adipose tissue is not due to the presence of the FGF receptor (FGFR) or β-klotho, since other tissues expressing these receptors can release FGF21 into the circulation, and deletion of β-klotho does not result in the appearance of circulating FGF21 in adipocyte-specific transgenic mice (our unpublished observations). Thus, adipose tissue responds particularly well to autocrine FGF21, suggesting that strategies to increase local production of the hormone may be more effective, with fewer side effects (67–70).

A second important question concerns the signaling pathway initiated by FGF21 in adipocytes required for induction of the thermogenic program. Amlexanox can elevate cAMP levels in adipocytes by blocking the phosphorylation and subsequent activation of cAMP phosphodiesterase 3B (27), representing the mechanism by which the expression and secretion of FGF21 and IL-6 are increased in response to the drug. Our findings indicate that FGF21 likely delivers a second signal required for activation of the thermogenic program by catecholamine signaling. Previous studies (71) have shown that β-adrenergic activation of adipocytes in vivo leads to increases in calcium-dependent pathways. We have recently shown that these pathways depend on the synthesis and secretion of FGF21 to provide and sustain this signal. However, it must be noted that other pathways may also be involved. Although FGF21 has long been known to activate the Ras/MAP kinase pathway (62, 72), this effect of the hormone is not required for induction of the thermogenic program. However, there may be other genes, such as Glut1 (73), that are controlled by this pathway and perhaps play a role in the biological effects of the hormone. Nevertheless, the importance of the autocrine actions of FGF21 on adipose tissue provides important insights into how this hormone can best be used as a therapeutic agent and suggests that strategies to increase adipocyte FGF21 synthesis with amlexanox or other TBK1/IKKε inhibitors might be beneficial.

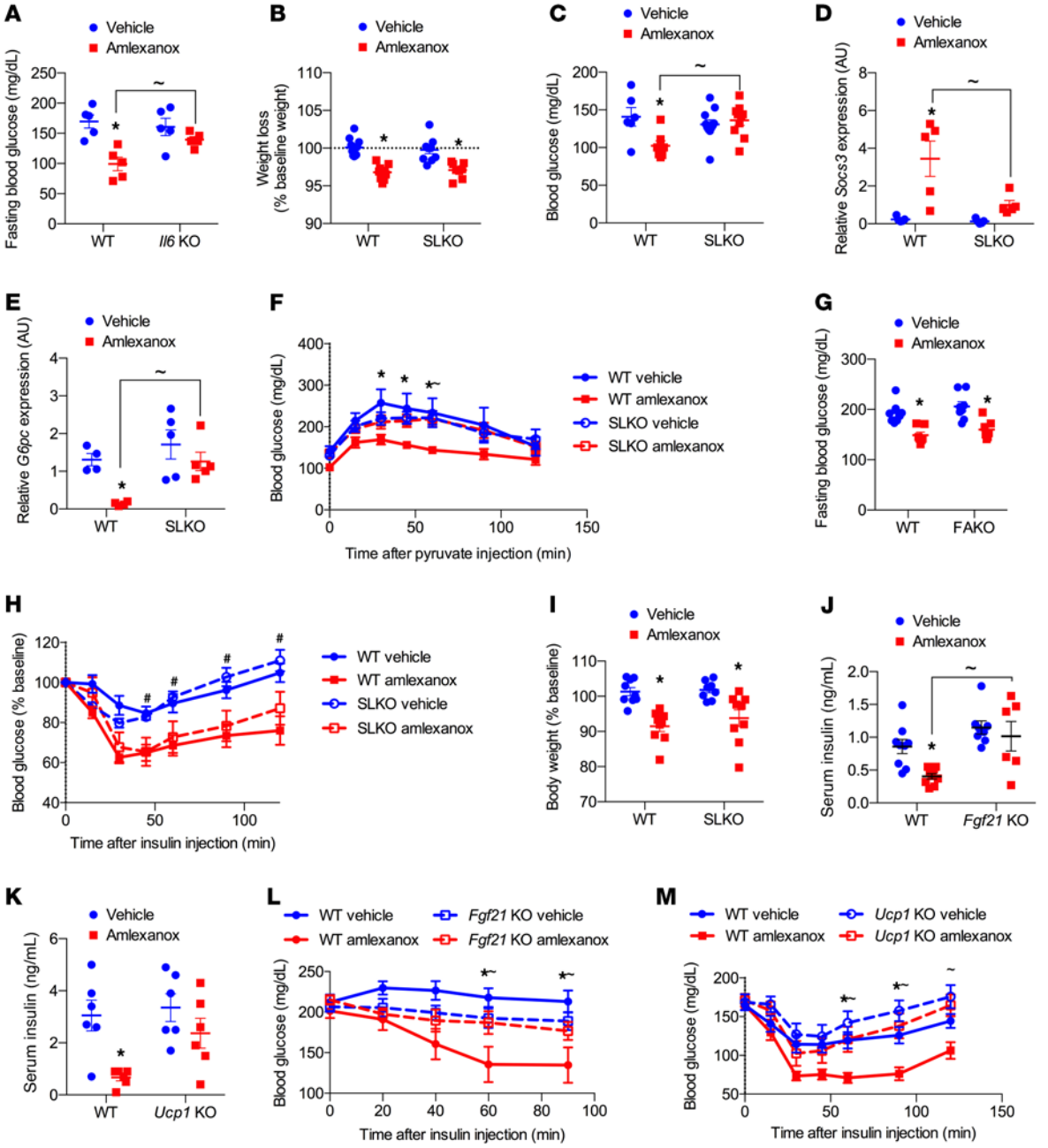

Figure 8. Mechanism of improved glucose handling and insulin sensitivity. (**A**) Day 3 fasting blood glucose levels in obese *Il6*-KO and WT littermate control mice. *n* = 5 animals per treatment per genotype. (**B**–**F**, **H**, and **I**) Obese SLKO and WT mice. (**B**) Day 3 weight loss. *n* = 10 vehicle-treated mice and *n* = 9 amlexanox-treated mice per genotype. (**C**) Day 3 fasting blood glucose levels. *n* = 6 vehicle-treated WT mice, *n* = 7 amlexanox-treated WT mice, *n* = 11 vehicle-treated SLKO mice, and *n* = 12 amlexanox-treated SLKO mice. Day 3 liver expression of (**D**) *Socs3* and (**E**) *G6pc*. *n* = 5 animals per genotype per treatment. (**F**) Pyruvate tolerance test after 3 days of treatment. *n* = 6 vehicle-treated WT mice, *n* = 7 amlexanox-treated WT mice, *n* = 11 vehicle-treated SLKO mice, and *n* = 12 amlexanox-treated SLKO mice. (**G**) Day 3 fasting blood glucose levels in obese FAKO and WT littermate control animals. *n* = 9 vehicle-treated mice and *n* = 8 amlexanox-treated mice per genotype. (**H**) Insulin tolerance test after 4 weeks of treatment. *n* = 8 vehicle-treated mice and *n* = 7 amlexanox-treated mice per genotype. (**I**) Weight loss after 4 weeks of treatment. *n* = 9 mice per treatment per genotype. (**J** and **K**) Fasting serum insulin levels in obese mice after 4 weeks of treatment. (**J**) Serum insulin levels in WT and *Fgf21*-KO mice. *n* = 9 WT mice per treatment, *n* = 8 vehicle-treated *Fgf21*-KO mice, and *n* = 6 amlexanox-treated *Fgf21*-KO mice. (**K**) Serum insulin levels in WT and *Ucp1*-KO mice. *n* = 6 mice per treatment per genotype. (**L**) Insulin tolerance test after 4 weeks of treatment in obese *Fgf21*-KO and WT littermate control mice. *n* = 10 vehicle-treated mice per genotype, *n* = 9 WT mice, and *n* = 8 amlexanox-treated *Fgf21*-KO mice. (**M**) Insulin tolerance test after 4 weeks of treatment in obese *Ucp1*-KO and WT littermate control mice. *n* = 10 vehicle-treated mice per genotype, *n* = 9 WT mice, and *n* = 8 amlexanox-treated *Ucp1*-KO mice. $^{*}P < 0.05$, by Holm-Šidák post hoc test after significant 2-way ANOVA for the vehicle versus amlexanox treatment groups. $^{\#}P < 0.05$, by Holm-Šidák post hoc test after significant 2-way ANOVA for vehicle versus amlexanox treatment in both the WT and KO groups. $^{\sim}P < 0.05$, by Holm-Šidák post hoc test after significant 2-way ANOVA for WT versus KO animals within the amlexanox treatment group. Data are presented as the mean ± SEM.

Methods

Animals

Whole-body–KO mice. Homozygous *Il6*-KO (stock no. 002650) and *Ucp1*-KO (stock no. 003124) mice were obtained from The Jackson Laboratory. These mice were bred with C57BL/6J mice (stock no. 000664) to generate heterozygous animals. Whole-body *Fgf21*–KO mice have been previously described (74). Cohorts of WT and KO littermate controls were generated from heterozygous-to-heterozygous breeding. Animals were genotyped prior to weaning, and WT and KO mice were cohoused after weaning.

Tissue-specific KO mice. Animals homozygous for the *Stat3*-floxed allele were obtained from The Jackson Laboratory (stock no. 016923). These mice were bred with *Alb* promoter–driven *Cre* mice (The Jackson Laboratory, stock no. 016832). The F1 generation was then intercrossed to generate mice homozygous for the *Stat3*-floxed allele both with (SLKO) and without (WT) the *Alb-Cre*. Cohorts were generated from the F2 generation and beyond. FLKO and FAKO mice expressing *Alb-Cre* and *Adipoq-Cre*, respectively, have been previously described (43).

All strains of mice were on a C57BL/6J background. Only male mice were used for the experiments. We fed mice a ND (Teklad, 7912). Obesity was induced by feeding animals a HFD consisting of 45% of calories from fat (Research Diets, D12451) for 12–13 weeks, starting at 6–10 weeks of age. Amlexanox was administered by daily oral gavage at a dose of 25 mg/kg. SB203,580 was administered by oral gavage at a dose of 20 mg/kg, 30–60 minutes prior to amlexanox administration. Mice were preconditioned to the oral gavage by at least 1 week of daily gavage with an equivalent volume of saline. During metabolic studies, ear tag numbers were used to identify animals. Within an experiment, genotype and/or treatment groups of mice were both littermates and cage mates. Researchers performing tests and collecting data were blinded to the treatment/genotype groups during the experiments. Animals in each cohort were produced from 20 breeding pairs to minimize the birth date range. Within each genotype, mice were assigned to treatment groups, such that prior to treatment the mean body weight, as well as the standard deviation of the body weight, was equal across treatment groups, using a method similar to block randomization. Additional consideration was given to housing, such that each cage contained multiple treatment groups, to avoid confounding by cage effects. Sample size was determined on the basis of available cohorts and the number of treatment groups required. Mice were housed in a specific pathogen–free facility under a 12-hour light/12-hour dark cycle and given free access to food and water, except for the fasting period.

Metabolic cage studies. For metabolic studies, the mice were subjected to a comprehensive laboratory monitoring system (CLAMS) (Columbus Instruments; CLAMS is an integrated open-circuit calorimeter equipped with an optical beam activity monitoring system) to measure the rates of oxygen consumption (VO_2) and carbon dioxide production (VCO_2) by indirect calorimetry and spontaneous motor activity at the University of Michigan's Metabolic Phenotyping Core, or at the ACP phenotyping core of UCSD for the paired feeding experiment.

Food intake and paired feeding. Food intake was measured by metabolic cages, or the weight of food provided was recorded, and then the remaining weight of the food was determined daily for singly housed mice. Pair-fed animals were provided the average amount food consumed by the control group, either by daily measured food provisions or automated feeder restrictions in metabolic cages.

Serum FGF21, IL-6, and insulin measurements. Blood was collected by submandibular bleeding and allowed to clot at room temperature for 30 minutes prior to serum isolation. IL-6 and FGF21 levels in 50 μL serum were measured using the Mouse IL-6 Quantikine ELISA (SM6000B) and the FGF21 Quantikine ELISA (MF2100) from R&D Systems. Serum insulin was measured in 2.5 μL serum with the Ultra-Sensitive Mouse Insulin ELISA Kit (Crystal Chem, catalog 90080).

Insulin and pyruvate tolerance tests. For insulin tolerance tests, mice were fasted for 3 hours and then given an intraperitoneal injection of 1.0 units of insulin per kilogram of body weight. For pyruvate tolerance tests, blood glucose levels from tail blood were measured after a 16-hour fast, using the OneTouch Ultra Glucometer (LifeScan). Mice were then given an intraperitoneal injection of sodium pyruvate (P2256) at a dose of 1.5 g/kg body weight. Blood was obtained from the tail, and blood glucose at basal levels and at 15, 30, 45, 60, 90, 120, and 180 minutes were measured using the OneTouch Ultra Glucometer (LifeScan).

Adipocyte size

Adipocyte size was assessed from H&E-stained WAT histology slides and imaged with a standard Texas red excitation and emission filter. Adipocyte size was measured using CellProfiler software (75). Objects that deviated from circularity were eliminated by omitting those objects with a form factor below 0.5 and an eccentricity above 0.95 for accurate identification of single adipocytes by the automated system. A minimum of 1000 cells from each animal were assayed.

Histology

Fat and liver tissues were collected and fixed in 10% formalin for 1 week and then placed in 70% ethanol. Paraffin embedment and sectioning for H&E staining and immunohistochemical analysis was completed at the UCSD Tissue Technology Core.

Western blot analysis

Tissues were homogenized in lysis buffer (50 mM Tris, pH 7.5, 150 mM NaCl, 4 mM EDTA, 10% glycerol, 1% Triton X-100, 1 mM DTT, 1 mM Na_3VO_4, 5 mM NaF, 1 mM phenylmethanesulfonylfluoride, 25 mM glycerol 2-phosphate and a freshly added protease inhibitor tablet) (Roche, 11836170001), followed by incubation for 1 hour at 4°C. Crude lysates were centrifuged twice at 17,000*g* for 15 minutes and the protein concentration determined using Bio-Rad Protein Assay Dye Reagent. Samples were diluted in SDS sample buffer. Bound proteins were resolved by SDS-PAGE and transferred onto nitrocellulose membranes (Bio-Rad). Individual proteins were detected with specific antibodies and visualized on film using HRP-conjugated secondary antibodies (Bio-Rad) and Western Lightning Enhanced Chemiluminescence (PerkinElmer Life Sciences). The following primary antibodies were used at a 1:1000 dilution unless otherwise specified and were purchased from Cell Signaling Technology: HSP90 (no. 4874), p705 STAT3 (no. 9131), STAT3 1:4000 (no. 9139), and AKT (no. 9272). Polyclonal goat anti-FGF21 antibody (catalog AF3057) was purchased from R&D Systems and used at a concentration of 1:500. Goat anti-mouse (no. 31430) and goat anti-rabbit (no. 31460) secondary antibodies were purchased from Thermo Fisher Scientific, and donkey anti-goat secondary antibody (catalog HAF109) was purchased from R&D Systems and used at a concentration of 1:10,000.

Cell culture

Primary preadipocytes were isolated from inguinal fat pads as follows: following fine mincing, the tissue was collagenase (2/mL mg/mL, MilliporeSigma, C6885) digested in a 37°C water bath with shaking for 15–20 minutes. FBS was added to 10%, and then the slurry was passed through a 100 μm filter and spun at 500*g* for 5 minutes. The cell pellet was washed once and plated in culture media with 2.5 mg/L amphotericin B (MilliporeSigma, A2411). Cells from the first and second passages were plated to confluence for experiments to ensure that all cells reached confluence at the same time. Differentiation was initiated with 500 μM 3-isobutyl-1-methylxanthine, 250 nM dexamethasone, 1 μg/mL insulin, and 1 μM troglitazone for 4 days, followed by insulin for 3 days. Cells were used for experiments 8 or 9 days after the initiation of differentiation. Only cultures in which greater than 90% of cells had adipocyte morphology were used. FGF21 and IL-6 secretion into media was quantified using the mouse IL-6 Quantikine ELISA (SM6000B) and FGF21 Quantikine ELISA (MF2100) from R&D Systems.

Reverse transcription PCR analysis of gene expression

RNA extractions from iWAT were performed using the RNeasy Lipid Tissue Kit (QIAGEN). The SuperScript First-Strand Synthesis System for reverse transcription PCR (RT-PCR) (Invitrogen, Thermo Fisher Scientific) was used with a 3:1 mixture of random hexamers and oligo-dT primers. RT-PCR amplification was performed on samples in triplicate with Power SYBR Green PCR Master Mix (Applied Biosystems) using the Applied Biosystems QuantStudio 5 real-time PCR System and quantified using an internal standard curve with *Arbp* as the control gene. The sequences of all primers used in this study are listed in Supplemental Table 1.

Statistics

When comparing the 2 groups, a 2-tailed, unpaired Student's *t* test was used to determine the significance of experimental results. For experiments with a 2-factorial design, 2-way ANOVA was performed to establish that not all groups were equal. Holm-Šidák post hoc analysis was then used for specific between-group comparisons after statistical significance was established by ANOVA. In each case, significance was set at $\alpha = 0.05$. Statistical analyses were performed using GraphPad Prism, version 6 (GraphPad Software).

Study approval

All animal experiments were approved by the IACUCs of UCSD and the University of Iowa.

Author contributions

SMR and ARS conceptualized the study. SMR, MAO, MA, MCN, NE, AVG, EW, BD, JHDL, and BP conducted formal analysis. SMR, MAO, MA, MCN, NE, AVG, EW, XP, BD, JHDL, and BP performed experiments. SMR, MAO, and XP designed the study methodology. MJP provided resources. SMR, MJP, and ARS supervised the study. SMR performed microscopy analysis. SMR wrote the original draft of the manuscript. SMR, MJP, and ARS reviewed and edited the manuscript.

Acknowledgments

We thank Steven A. Kliewer and David J. Mangelsdorf for providing the *Fgf21* whole-body and liver-specific–KO mouse strains. We thank members of the Saltiel laboratory for helpful discussions, comments, and suggestions. We thank the UCSD histology core for tissue sectioning and staining. We thank Eunice J. Choi for running CellProfiler to determine adipocyte size. This work was supported by the American Diabetes Association (1-19-JDF-012, to SMR and 1-19-PDF-177, to MA). This work was also supported by the NIH (F32DK09685101, 1K01DK105075, and R03DK118195, to SMR; R01DK106104, to MJP; and P30 DK063491, R01DK117551, R01DK125820, and R01DK076906, to ARS).

Address correspondence to: Alan R. Saltiel, UCSD, 9452 Medical Center Drive, ACTRI-L1E210, La Jolla, California 92037, USA. Phone: 858.534.5953; Email: asaltiel@health.ucsd.edu. MA's present address is: Department of Molecular Physiology and Biophysics, Vanderbilt University Nashville, Nashville, Tennessee 37240, USA. BP's present address is: Department of Radiology, University of Texas Southwestern Medical Center, Dallas, Texas 75390, USA. EW's present address is: Explora Biolabs, San Diego, California 92121, USA.

1. James PT, et al. The worldwide obesity epidemic. *Obes Res*. 2001;9(Suppl 4):228S–233S.
2. No authors listed. Obesity: preventing and managing the global epidemic. Report of a WHO consultation. *World Health Organ Tech Rep Ser*. 2000;894:1–253.
3. Swinburn BA, et al. The global obesity pandemic: shaped by global drivers and local environments. *Lancet*. 2011;378(9793):804–814.
4. Knowler WC, et al. Diabetes mellitus in the Pima Indians: incidence, risk factors and pathogenesis. *Diabetes Metab Rev*. 1990;6(1):1–27.
5. Zimmet P. Epidemiology of diabetes and its macrovascular manifestations in Pacific populations: the medical effects of social progress. *Diabetes Care*. 1979;2(2):144–153.
6. O'Neill S, O'Driscoll L. Metabolic syndrome: a closer look at the growing epidemic and its associated pathologies. *Obes Rev*. 2015;16(1):1–12.
7. Biddinger SB, Kahn CR. From mice to men: insights into the insulin resistance syndromes. *Annu Rev Physiol*. 2006;68:123–158.
8. Olefsky JM, Glass CK. Macrophages, inflammation, and insulin resistance. *Annu Rev Physiol*. 2010;72:219–246.
9. Lumeng CN, Saltiel AR. Inflammatory links between obesity and metabolic disease. *J Clin Invest*. 2011;121(6):2111–2117.
10. Gregor MF, Hotamisligil GS. Inflammatory mechanisms in obesity. *Annu Rev Immunol*. 2011;29:415–445.
11. Shoelson SE, et al. Inflammation and insulin resistance. *J Clin Invest*. 2006;116(7):1793–1801.
12. Fujisaka S, et al. Regulatory mechanisms for adipose tissue M1 and M2 macrophages in diet-induced obese mice. *Diabetes*. 2009;58(11):2574–2582.
13. Lumeng CN, et al. Increased inflammatory properties of adipose tissue macrophages recruited during diet-induced obesity. *Diabetes*. 2007;56(1):16–23.
14. Lumeng CN, et al. Macrophages block insulin action in adipocytes by altering expression of signaling and glucose transport proteins. *Am J Physiol Endocrinol Metab*. 2007;292(1):E166–E174.
15. Reilly SM, Saltiel AR. Adapting to obesity with adipose tissue inflammation. *Nat Rev Endocrinol*. 2017;13(11):633–643.
16. Hotamisligil GS. Inflammation and metabolic disorders. *Nature*. 2006;444(7121):860–867.
17. Saltiel AR, Olefsky JM. Inflammatory mechanisms linking obesity and metabolic disease. *J Clin Invest*. 2017;127(1):1–4.
18. Baker RG, et al. NF-κB, inflammation, and metabolic disease. *Cell Metab*. 2011;13(1):11–22.
19. Wunderlich FT, et al. Hepatic NF-kappa B essential modulator deficiency prevents obesity-induced insulin resistance but synergizes with high-fat feeding in tumorigenesis. *Proc Natl Acad Sci U S A*. 2008;105(4):1297–1302.
20. Arkan MC, et al. IKK-beta links inflammation to obesity-induced insulin resistance. *Nat Med*. 2005;11(2):191–198.
21. Reilly SM, et al. An inhibitor of the protein kinases TBK1 and IKK-ε improves obesity-related metabolic

dysfunctions in mice. *Nat Med*. 2013;19(3):313–321.
22. He Q, et al. Long-term subcutaneous injection of lipopolysaccharides and high-fat diet induced non-alcoholic fatty liver disease through IKKepsilon/NF-kappaB signaling. *Biochem Biophys Res Commun*. 2020;532(3):362–369.
23. Zhao P, et al. TBK1 at the crossroads of inflammation and energy homeostasis in adipose tissue. *Cell*. 2018;172(4):731–743.
24. Chiang SH, et al. The protein kinase IKKepsilon regulates energy balance in obese mice. *Cell*. 2009;138(5):961–975.
25. Makino H, et al. Mechanism of action of an anti-allergic agent, amlexanox (AA-673), in inhibiting histamine release from mast cells. Acceleration of cAMP generation and inhibition of phosphodiesterase. *Int Arch Allergy Appl Immunol*. 1987;82(1):66–71.
26. Oral EA, et al. Inhibition of IKKε and TBK1 improves glucose control in a subset of patients with type 2 diabetes. *Cell Metab*. 2017;26(1):157–170.
27. Mowers J, et al. Inflammation produces catecholamine resistance in obesity via activation of PDE3B by the protein kinases IKKε and TBK1. *Elife*. 2013;2:e01119.
28. Li M, et al. TNF-α upregulates IKKε expression via the Lin28B/let-7a pathway to induce catecholamine resistance in adipocytes. *Obesity (Silver Spring)*. 2019;27(5):767–776.
29. Reilly SM, et al. A subcutaneous adipose tissue-liver signalling axis controls hepatic gluconeogenesis. *Nat Commun*. 2015;6:6047.
30. Timper K, et al. IL-6 improves energy and glucose homeostasis in obesity via enhanced central IL-6 trans-signaling. *Cell Rep*. 2017;19(2):267–280.
31. Le Foll C, et al. Amylin-induced central IL-6 production enhances ventromedial hypothalamic leptin signaling. *Diabetes*. 2015;64(5):1621–1631.
32. Wallenius K, et al. Intracerebroventricular interleukin-6 treatment decreases body fat in rats. *Biochem Biophys Res Commun*. 2002;293(1):560–565.
33. Liu J, et al. An evaluation on the efficacy and safety of amlexanox oral adhesive tablets in the treatment of recurrent minor aphthous ulceration in a Chinese cohort: a randomized, double-blind, vehicle-controlled, unparallel multicenter clinical trial. *Oral Surg Oral Med Oral Pathol Oral Radiol Endod*. 2006;102(4):475–481.
34. Hariya T, et al. Allergenicity and tolerogenicity of amlexanox in the guinea pig. *Contact Dermatitis*. 1994;31(1):31–36.
35. Fisher FM, et al. FGF21 regulates PGC-1α and browning of white adipose tissues in adaptive thermogenesis. *Genes Dev*. 2012;26(3):271–281.
36. Huang Z, et al. The FGF21-CCL11 axis mediates beiging of white adipose tissues by coupling sympathetic nervous system to type 2 immunity. *Cell Metab*. 2017;26(3):493–508.
37. Neinast MD, et al. Activation of natriuretic peptides and the sympathetic nervous system following Roux-en-Y gastric bypass is associated with gonadal adipose tissues browning. *Mol Metab*. 2015;4(5):427–436.
38. Fabbiano S, et al. Caloric restriction leads to browning of white adipose tissue through type 2 immune signaling. *Cell Metab*. 2016;24(3):434–446.
39. Yoda T, et al. Effects of food deprivation on daily changes in body temperature and behavioral thermoregulation in rats. *Am J Physiol Regul Integr Comp Physiol*. 2000;278(1):R134–R139.
40. Swoap SJ. The pharmacology and molecular mechanisms underlying temperature regulation and torpor. *Biochem Pharmacol*. 2008;76(7):817–824.
41. Soare A, et al. Long-term calorie restriction, but not endurance exercise, lowers core body temperature in humans. *Aging (Albany NY)*. 2011;3(4):374–379.
42. Nishimura T, et al. Identification of a novel FGF, FGF-21, preferentially expressed in the liver. *Biochim Biophys Acta*. 2000;1492(1):203–206.
43. Markan KR, et al. Circulating FGF21 is liver derived and enhances glucose uptake during refeeding and overfeeding. *Diabetes*. 2014;63(12):4057–4063.
44. Inagaki T, et al. Endocrine regulation of the fasting response by PPARalpha-mediated induction of fibroblast growth factor 21. *Cell Metab*. 2007;5(6):415–425.
45. Galman C, et al. The circulating metabolic regulator FGF21 is induced by prolonged fasting and PPARalpha activation in man. *Cell Metab*. 2008;8(2):169–174.
46. Coate KC, et al. FGF21 is an exocrine pancreas secretagogue. *Cell Metab*. 2017;25(2):472–480.
47. Chartoumpekis DV, et al. Brown adipose tissue responds to cold and adrenergic stimulation by induction of FGF21. *Mol Med*. 2011;17(7–8):736–740.
48. Lee P, et al. Mild cold exposure modulates fibroblast growth factor 21 (FGF21) diurnal rhythm in humans: relationship between FGF21 levels, lipolysis, and cold-induced thermogenesis. *J Clin Endocrinol Metab*. 2013;98(1):E98–102.
49. Wiejak J, et al. Extracellular signal-regulated kinase mitogen-activated protein kinase-dependent SOCS-3 gene induction requires c-Jun, signal transducer and activator of transcription 3, and specificity protein 3 transcription factors. *Mol Pharmacol*. 2012;81(5):657–668.
50. Yang J, et al. Reversible methylation of promoter-bound STAT3 by histone-modifying enzymes. *Proc Natl Acad Sci U S A*. 2010;107(50):21499–21504.
51. Isobe A, et al. STAT3-mediated constitutive expression of SOCS3 in an undifferentiated rat trophoblast-like cell line. *Placenta*. 2006;27(8):912–918.
52. Ramadoss P, et al. STAT3 targets the regulatory regions of gluconeogenic genes in vivo. *Mol Endocrinol*. 2009;23(6):827–837.
53. Inoue H, et al. Role of STAT-3 in regulation of hepatic gluconeogenic genes and carbohydrate metabolism in vivo. *Nat Med*. 2004;10(2):168–174.
54. Inoue H, et al. Role of hepatic STAT3 in brain-insulin action on hepatic glucose production. *Cell Metab*. 2006;3(4):267–275.
55. Saltiel AR. New therapeutic approaches for the treatment of obesity. *Sci Transl Med*. 2016;8(323):323rv2.
56. Li P, et al. Functional heterogeneity of CD11c-positive adipose tissue macrophages in diet-induced obese mice. *J Biol Chem*. 2010;285(20):15333–15345.
57. Zatterale F, et al. Chronic adipose tissue inflammation linking obesity to insulin resistance and type 2 diabetes. *Front Physiol*. 2019;10:1607.
58. Weissmann L, et al. IKKε is key to induction of insulin resistance in the hypothalamus, and its inhibition reverses obesity. *Diabetes*. 2014;63(10):3334–3345.
59. Campolim CM, et al. Short-term exposure to air pollution ($PM_{2.5}$) induces hypothalamic inflammation, and long-term leads to leptin resistance and obesity via Tlr4/Ikbke in mice. *Sci Rep*. 2020;10(1):10160.
60. Jais A, Bruning JC. Hypothalamic inflammation in obesity and metabolic disease. *J Clin Invest*. 2017;127(1):24–32.
61. Kazak L, et al. UCP1 deficiency causes brown fat respiratory chain depletion and sensitizes mitochondria to calcium overload-induced dysfunction. *Proc Natl Acad Sci U S A*. 2017;114(30):7981–7986.
62. Tezze C, et al. FGF21 as modulator of metabolism in health and disease. *Front Physiol*. 2019;10:419.
63. Markan KR, Potthoff MJ. Metabolic fibroblast growth factors (FGFs): Mediators of energy homeostasis. *Semin Cell Dev Biol*. 2016;53(FGFs):85–93.
64. Kliewer SA, Mangelsdorf DJ. A dozen years of discovery: insights into the physiology and pharmacology of FGF21. *Cell Metab*. 2019;29(2):246–253.
65. BonDurant LD, Potthoff MJ. Fibroblast growth factor 21: a versatile regulator of metabolic homeostasis. *Annu Rev Nutr*. 2018;38:173–196.
66. Goetz R, et al. Molecular insights into the klotho-dependent, endocrine mode of action of fibroblast growth factor 19 subfamily members. *Mol Cell Biol*. 2007;27(9):3417–3428.
67. Wei W, et al. Fibroblast growth factor 21 promotes bone loss by potentiating the effects of peroxisome proliferator-activated receptor γ. *Proc Natl Acad Sci U S A*. 2012;109(8):3143–3148.
68. Talukdar S, et al. A long-acting FGF21 molecule, PF-05231023, decreases body weight and improves lipid profile in non-human primates and type 2 diabetic subjects. *Cell Metab*. 2016;23(3):427–440.
69. Wang X, et al. A liver-bone endocrine relay by IGFBP1 promotes osteoclastogenesis and mediates FGF21-induced bone resorption. *Cell Metab*. 2015;22(5):811–824.
70. Charoenphandhu N, et al. Fibroblast growth factor-21 restores insulin sensitivity but induces aberrant bone microstructure in obese insulin-resistant rats. *J Bone Miner Metab*. 2017;35(2):142–149.
71. Ikeda K, et al. UCP1-independent signaling involving SERCA2b-mediated calcium cycling regulates beige fat thermogenesis and systemic glucose homeostasis. *Nat Med*. 2017;23(12):1454–1465.
72. Xu Z, et al. The role of ERK1/2 in the development of diabetic cardiomyopathy. *Int J Mol Sci*. 2016;17(12):E2001.
73. Ge X, et al. Fibroblast growth factor 21 induces glucose transporter-1 expression through activation of the serum response factor/Ets-like protein-1 in adipocytes. *J Biol Chem*. 2011;286(40):34533–34541.
74. Potthoff MJ, et al. FGF21 induces PGC-1alpha and regulates carbohydrate and fatty acid metabolism during the adaptive starvation response. *Proc Natl Acad Sci U S A*. 2009;106(26):10853–10858.
75. MacDougald OA. Methods in enzymology. Methods of adipose tissue biology, part B. preface. *Methods Enzymol*. 2014;538:xv.